

<https://doi.org/10.1038/s43247-023-00922-2>

OPEN

Soil moisture–atmosphere feedbacks have triggered the shifts from drought to pluvial conditions since 1980

Yamin Qing ^{1,4}, Shuo Wang ^{1,4}✉, Zong-Liang Yang ² & Pierre Gentine ³

Drought and pluvial transitions have attracted widespread attention. However, the dynamic evolution and underlying mechanisms of drought and pluvial transitions remain poorly understood. Here, we demonstrate that there is a significant increase in the occurrence of drought and pluvial transitions (0.24–1.03% per year) globally during 1980–2020. We use convergent cross mapping to detect causal relationships between time series variables in the climate system and find that drought and pluvial transitions can be explained by an indirect transitive causal chain. Specifically, the soil moisture–latent heat flux–precipitation causal chain is likely to trigger the rainfall following the dryness in humid regions where enhanced evaporation increases the actual atmospheric moisture favoring the pluvial occurrence. By contrast, the soil moisture–moisture convergence–precipitation causal chain enhances the post-drought rainfall in arid regions due to atmospheric circulation dynamics. Our results indicate that land–atmosphere feedbacks play an important role in triggering the drought–pluvial shift in a changing climate.

¹Department of Land Surveying and Geo-Informatics, Research Institute for Land and Space, The Hong Kong Polytechnic University, Hong Kong, China.

²Department of Geological Sciences, The John A. and Katherine G. Jackson School of Geosciences, University of Texas at Austin, Austin, TX, USA.

³Department of Earth and Environmental Engineering, Columbia University, New York, NY 10027, USA. ⁴These authors contributed equally: Yamin Qing, Shuo Wang. ✉email: shuo.s.wang@polyu.edu.hk

Droughts are linked to prolonged periods of low precipitation and/or dry soils, whereas pluvials often refer to the periods of enhanced and intense precipitation^{1,2}. Drought and pluvial have a substantial influence on available water resources and agricultural productivity^{3–5}. The transitions from drought to pluvial may lead to greater impacts than the sum of individual events due to the potential increase in the vulnerability of populations and ecosystems². Furthermore, more attention should be paid to the drought to pluvial transitions that have compound effects as droughts make the area more vulnerable to the following pluvials. For example, the middle to low reaches of the Yangtze River was hit by abrupt drought-pluvial transitions in 2011⁶. The 2015 growing season across the south-central United States was characterized by an unusual sequence of events that saw parts of the region flipping from extreme drought conditions to a pluvial during spring⁷. In September 2015, there was a fast transition from drought to pluvial flooding within 1 week over South Carolina of United States, which brought a once-in-a-thousand-years flood². In addition, Texas experienced the worst drought during 2011–2015, which was suddenly ended by a heavy rainfall event in spring 2015. Such heavy rainfall event caused flash flooding, which already significantly changed the landscape, vegetation distribution and soil infiltration properties^{2,8}. These recent examples of successive drought and pluvial highlight their compound impacts, pointing to a more variable and extreme climate^{9–11}. Thus, there is a need to reveal the dynamic evolution and underlying mechanisms of drought and pluvial transitions, especially the abrupt transition, advancing our understanding of such an abrupt transition on a global scale and providing meaningful information to increase society's resilience to the swings from drought to pluvial.

Global Land–Atmosphere Coupling Experiments (GLACE) have identified the regions where soil moisture may have a strong impact on precipitation variability in earlier generation of climate models^{12,13}. Findell et al.¹⁴ found that high evaporation enhanced the probability of afternoon rainfall over eastern U.S. and Mexico, and this result is similar to those found by D'Odorico and Porporato¹⁵ over Illinois. Ruiz-Barradas and Nigam¹⁶ found that remote moisture sources were more important than local evaporation for precipitation variability over the U.S. Great Plains, and argued against the strong soil moisture–precipitation feedback found in some modeling studies. Thus, soil moisture affects the following precipitation through both local evaporation and remote moisture transport^{17,18}. However, the direct relationship between soil moisture and precipitation is complex, and varies in signal and strength due to the complex interactions between hydrological and climatic factors. On the other hand, soil moisture is involved in a number of dynamic feedbacks at the local, regional and global scales, and plays a dominant role in regulating climate change and extremes^{19–21}. Instead of investigating the soil moisture–precipitation coupling, we elucidate the causal pathways in the process chain of land–atmosphere feedbacks triggering the transition between drought and pluvial, thereby potentially improving predictions of extreme events for better adaptation and planning.

According to the Intergovernmental Panel on Climate Change (IPCC)'s Sixth Assessment Report (AR6)²², many regions around the world are projected to experience an increase in the probability of compound events (two or more extreme events occurring simultaneously or successively) with higher global warming, stressing the need to further explore the mechanism behind compound events. Considerable efforts have been made to detect individual drought and pluvial as well as their compound events regionally and globally over the past several years^{23–31}. However, little effort has been made to uncover the mechanism behind the drought and pluvial transitions (DPTs), especially from the

perspective of soil moisture–atmosphere feedbacks. Previous studies have indicated that soil moisture–atmosphere feedbacks initiated by soil moisture anomalies can strongly modulate rainfall, heat, and aridity locally^{32,33}, and can also promote large-scale atmospheric circulation anomalies remotely^{34,35}, which may contribute to the active/break phase transition of drought and pluvial. Given the importance of soil moisture–atmosphere feedbacks in the hydrological cycle, it is crucial to systematically investigate the role of soil moisture in the occurrence of DPTs.

Here, we first investigate the global pattern of DPTs and their spatiotemporal variations during the period of 1980–2020, based on the observationally constrained soil moisture and precipitation obtained from the ERA5, MERRA-2, and GLEAM datasets. Additionally, we explore the mechanisms behind the DPT occurrence from the perspective of soil moisture–atmosphere feedbacks. Our findings highlight an increasing risk of DPTs and indicate that land–atmosphere interactions may play an important role in triggering the shift from drought to pluvial in a changing climate.

Results

Mechanisms underlying the occurrence of DPTs. Drought and pluvial are associated with atmospheric circulation induced by local- and large-scale climate anomalies, and soil moisture–atmosphere feedbacks have been suggested to play a central role in the evolution of atmospheric circulation anomalies across time scales^{36–38}. Here, we focus on the contrasting role of soil moisture–atmosphere feedbacks in regulating the occurrence of DPTs. Soil moisture–atmosphere feedbacks are initiated by soil moisture anomalies, inducing land evaporation and surface heat flux anomalies that may trigger moisture convergence and further increase the likelihood of post-drought rainfall.

Water vapor for post-drought rainfall comes from both local evaporation and remote moisture transport, which can be modulated by a chain of processes resulting from land–atmosphere feedbacks. Figure 1 shows the land–atmosphere feedbacks as local and remote intensifiers of the post-drought rainfall. The latent heat flux in the surface energy balance directly relates to evaporation to moisten the atmosphere, which is the main local moisture resource. When soil and vegetation dry out, the air becomes even hotter, and warmer conditions during drought are often more favorable for evaporation, especially in humid regions. Additionally, the surface soil drying causes the increase in sensible heat flux, and vegetation accessing deeper soil moisture/groundwater is able to supply the water for evaporation in hotter environment, which in turn enhance the evaporative demand and thus potentially the surface latent heat flux, increasing atmospheric moisture content. Further, the atmospheric water-holding capacity enhanced by increasing temperature due to more partitioning of energy towards sensible heat allows air to hold more moisture under global warming. Thus, the increasing atmospheric moisture content, along with enhanced atmospheric water-holding capacity, indicates that the actual atmospheric moisture content should increase, leading potentially to the occurrence of rainfall, even heavy rainfall (Fig. 1a). Like the sharp turn from drought to flood that occurred in the middle and lower reaches of the Yangtze River in the early summer of 2011, the above-average latent heat flux was captured during the month before the occurrence of rainfall (Supplementary Fig. 1). On the other hand, atmospheric moisture convergence is a remote source of moisture for precipitation. Especially in dry areas, soil moisture limits evaporation and reduces moisture recycling for precipitation, but the reduced soil moisture also enhances moisture convergence which plays a more important role in the occurrence of heavier rainfall³⁹ (Fig. 1b). For example, severe drought

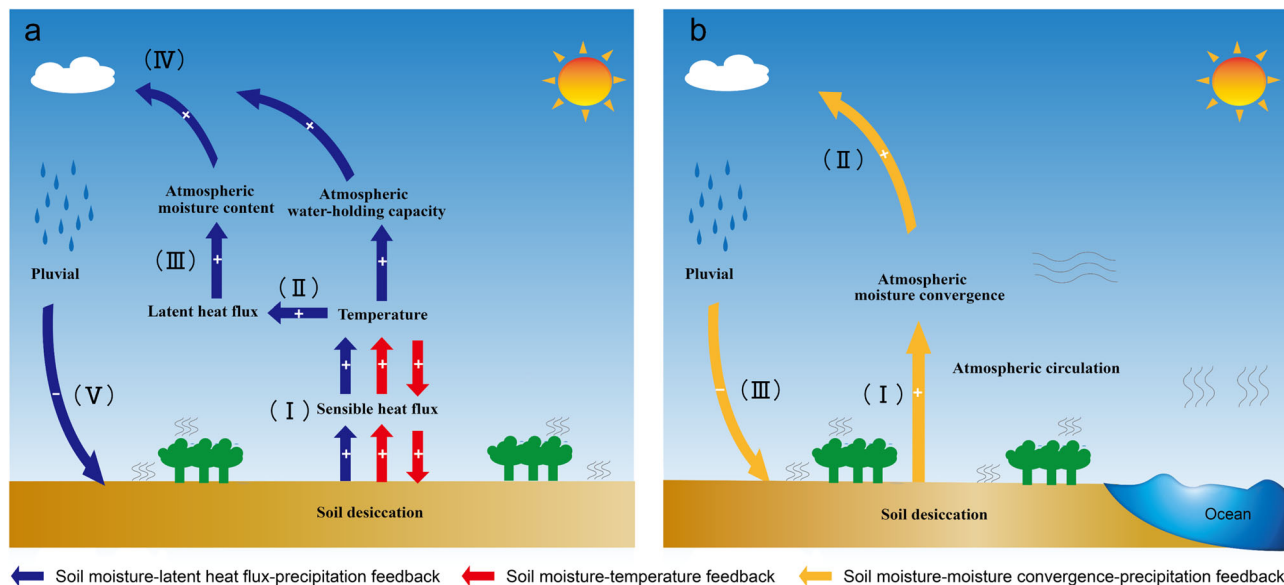


Fig. 1 Proposed mechanism for explaining the shift from drought to pluvial from the perspective of soil moisture–atmosphere feedbacks. Here, plus (+) and minus (–) indicate positive and negative relations, respectively. The colors show the soil moisture–latent heat flux–precipitation (blue), the soil moisture–temperature (red) and the soil moisture–moisture convergence–precipitation (yellow) feedback loops. **a** Local moisture transport processes: (I) Soil desiccation increases sensible heat flux, and the increasing sensible heat flux further enhances temperature. (II) Hotter air in turn enhances the evaporative demand and thus latent heat flux if water is sufficient. (III) As latent heat flux and temperature rise, atmospheric water-holding capacity and moisture content increase. (IV) Pluvial is likely to be triggered by the increase in actual atmospheric moisture content. (V) Pluvial prevents further soil desiccation. **b** Remote moisture transport processes: (I) Soil desiccation enhances low-level flow convergence to increase moisture. (II) As moisture in air rises, pluvial is likely to be triggered. (III) Pluvial prevents further soil desiccation. Ocean is the main moisture source in the remote moisture transport processes.

occurred over southeastern Australia in 2009, and was then terminated by a rainfall during 2010. At the end of drought, much higher than normal moisture convergence was observed before the occurrence of rainfall (Supplementary Fig. 2). Therefore, the changes in latent heat flux (land evaporation) and moisture convergence as well as their interactions with soil moisture may play an important role in triggering the shift from drought to pluvial. Although the soil moisture–precipitation feedback is complex, the indirect chain of processes resulting from land–atmosphere feedbacks (i.e., soil moisture–latent heat flux–precipitation and soil moisture–moisture convergence–precipitation) may help us to understand why drought and pluvial often occur in a consecutive order.

Observed changes in the characteristics of DPTs. Here we use three observationally constrained ERA5, MERRA-2, and GLEAM reanalysis products to increase the robustness of DPT analysis. We use the standardized soil moisture index (SSI < –1) based on soil moisture to define drought (soil moisture deficit) and the standardized precipitation index (SPI > 1) based on precipitation to define pluvial for different reanalysis datasets.

Figure 2 shows the spatial pattern of the frequency of DPTs for a recent warming period of 1980–2020, corresponding to the three different datasets used in this study. We highlight that the high frequency of DPT events is not a coincidence by performing the Superposed Epoch analysis, and we find that the precipitation response to drought is significant in more than two-thirds (at 95% confidence level) and half (at 99% confidence level) of the world’s regions (Supplementary Figs. 3 and 4). DPTs are more frequent over eastern North America, Europe, East Asia, Southeast Asia, southern Australia, southern Africa, and southern South America (Fig. 2a–d). Similar hotspots of the DPTs frequency can also be found by using different thresholds of indices (Supplementary Fig. 5). We examine the interannual

changes in the global mean frequency of DPTs, estimated as the mean value of grid cells that witness the DPTs during the period of 1980–2020. Even though different reanalysis datasets are used in this study, the results show a consistent trend for the ERA5, MERRA-2, and GLEAM datasets, especially a huge increasing trend for ERA5. There is a significant increase in the frequency (0.24–1.03% year^{–1}) of DPTs globally during the recent period of 1980–2020 (Fig. 2e). The global mean frequency during the period of 2001–2020, is larger than that observed during the period of 1981–2000 (Fig. 2f). Further, although spatial distribution of DPTs frequency varies for DJF, JJA, MAM, and SON, they all show a significant increasing trend during the period of 1980–2020 (Supplementary Fig. 6). And most subregions show a relatively consistent trend for DJF, JJA, MAM, and SON (Supplementary Fig. 7). Specifically, wet regions (i.e., humid and transitional regions) witness a higher increase in the frequency compared with arid regions (inconsistent trends from three datasets) (Supplementary Fig. 8). Significant increasing trends in the global mean frequency of DPTs are also detected through other time-series based modeling (i.e., assuming a Poisson process time series analysis based on soil moisture and precipitation percentiles) (Supplementary Figs. 9 and 10).

Possible coupling chains triggering the occurrence of DPTs.

The partial negative correlation of soil moisture and precipitation as well as the significant response of rainfall to drought occurrence all suggest that the lower soil moisture is likely to be followed by heavier precipitation (Supplementary Figs. 4 and 11). To investigate the role of soil moisture–atmosphere feedbacks in the occurrence and variation of DPTs, we use a probability multiplication factor (PMF) to assess the increase in the joint probability of occurrence of DPTs, compared to the probability expected if drought and pluvial were independent (i.e., the increase is due to the fact that the events are compound events).

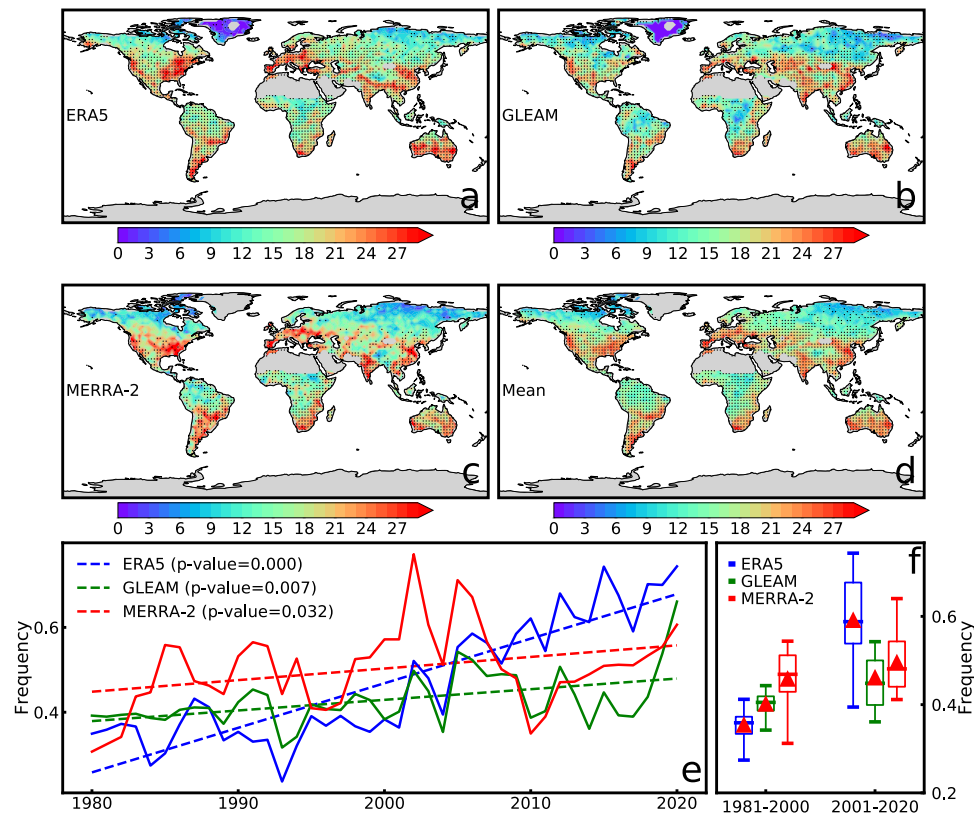


Fig. 2 Spatiotemporal pattern of the total number of DPTs during the period of 1980–2020. Spatial pattern of the total number of DPTs for each pixel during the period of 1980–2020 based on **a** ERA5, **b** MERRA-2, and **c** GLEAM datasets. **d** Spatial pattern of the multi-model mean number of DPTs for each pixel during the period of 1980–2020. Stippling denotes the regions where the frequency is statistically significant at the 99% level based on Superposed Epoch Analysis (SEA). **e** Annual time series (solid lines) of globally averaged DPTs over the regions where the DPT frequency passes the significance test. The linear annual trends (dashed lines) for ERA5, MERRA-2, and GLEAM are estimated based on the Sen's slope estimator, and statistical significances in trends are determined based on the MK test for 1980–2020. **f** Box plots of the total number of DPTs for each pixel during the periods of 1981–2000 and 2001–2020. The short horizontal line inside the box represents the 50th percentile, and the top and bottom of the box represent the 75th and 25th percentiles, respectively. The top and bottom of the line represent the 5th and 95th percentiles, respectively. The red triangles represent the mean values.

The joint probability of occurrence of DPTs is defined as a sequential occurrence of drought and pluvial when the soil moisture is below its 15th percentile and the post-drought precipitation is above its 85th percentile (15th percentile is approximately equal to the SSI value of -1 and the 85th percentile is approximately equal to the SPI value of 1).

We find that the PMF values of DPTs and the consistent negative soil moisture–latent heat flux couplings are mostly stronger in wet regions (i.e., humid and transitional regions) (Fig. 3a–f). Specifically, the hotspots of negative soil moisture–latent heat flux couplings are mostly located in Europe and eastern North America for all three datasets, indicating that the soil moisture–latent heat flux–precipitation coupling chain may be the transitive processes behind the influence of soil moisture on precipitation, which is likely to play a role in the occurrence of DPTs in wet regions, especially when there is a significant positive correlation between latent heat flux and precipitation (Supplementary Fig. 12). It is well understood that the occurrence of rainfall is associated with an increased latent heat flux (evaporation) at the Earth surface. In addition, greenhouse warming enhances the intensity of rainfall^{40–42} since the increasing temperature accompanied by an increase in latent heat flux (evaporation). Further, the increased water-holding capacity of the atmosphere and, together with an enhanced evaporation, lead to an increase in the actual atmospheric moisture. Eventually, the increased moisture content of the atmosphere favors rainfall events, as is observed to be occurring

in many parts of the world, thereby leading to an increasing risk of DPTs.

Our findings demonstrate that the PMF values of DPTs and the negative soil moisture–moisture convergence feedbacks are mostly stronger in dry regions (i.e., arid regions) (Fig. 3g–i), suggesting that the soil moisture–moisture convergence–precipitation coupling chain may be the dominant transitive processes behind the influence of soil moisture on precipitation in dry regions when moisture convergence and precipitation are significantly positively correlated (Supplementary Fig. 13). The reduced soil moisture enhances surface heating, thereby promoting the vertical ascent and associated low-level flow convergence. Furthermore, we find that the negative soil moisture feedback on mean flow convergence arises principally from both dynamic and thermodynamic components (Supplementary Fig. 14). This indicates that the negative soil moisture–moisture convergence feedback is mainly determined by the soil moisture regulation of atmospheric circulation, and the decreased soil moisture regulates the atmospheric circulation that can bring much moisture from remote moisture fluxes. Although the soil moisture–moisture convergence coupling plays a dominant role in the occurrence of DPTs in dry regions, the increased latent heat caused by the increase in the turbulent energy (latent plus sensible heat) transferred from the surface to the atmosphere under the influence of anthropogenic climate change is also a contributor, which can lead to increased air moisture and thus increased rainfall intensity⁴³.

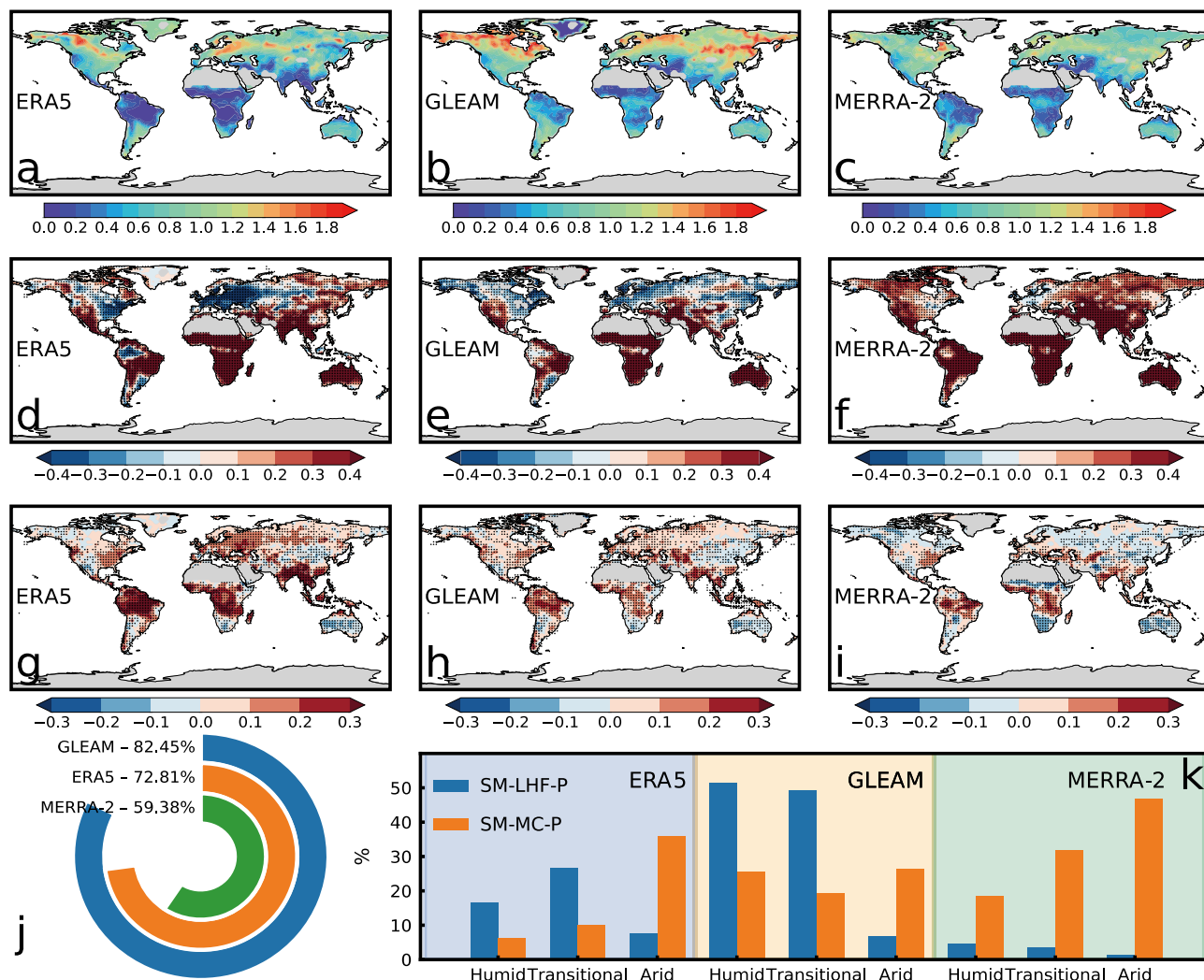


Fig. 3 Relationship between soil moisture (SM) and atmospheric factors (i.e., latent heat flux (LHF), moisture convergence (MC), and precipitation (P)) for ERA5, MERRA-2, and GLEAM datasets. Mean PMF of concurrent drought (soil moisture below the 15th percentile) and next-pentad pluvial (precipitation above the 85th percentile) over the period of 1980–2020 based on **a** ERA5, **b** GLEAM, and **c** MERRA-2 datasets. Correlation of mean soil moisture and next-pentad latent heat flux over the period of 1980–2020 based on **d** ERA5, **e** GLEAM, and **f** MERRA-2 datasets. Correlation of mean soil moisture and next-pentad moisture convergence over the period of 1980–2020 based on **g** ERA5, **h** GLEAM, and **i** MERRA-2 datasets. **j** Percentage of areas with significant soil moisture–latent heat flux–precipitation and soil moisture–moisture convergence–precipitation transitive chains over the areas with high probability of concurrent drought and next-pentad pluvial (PMF > 1). **k** Percentage of areas with significant soil moisture–latent heat flux–precipitation and soil moisture–moisture convergence–precipitation transitive chains over the humid, transitional, and arid areas for ERA5, GLEAM, and MERRA-2 datasets. Stippling represents the regions where the correlation between soil moisture–latent heat flux and soil moisture–moisture convergence is statistically significant at the level of 0.01.

The regions with significant soil moisture–latent heat flux–precipitation and soil moisture–moisture convergence–precipitation transitive chains account for 59.38–82.45% of the regions with higher probability of occurrence of DPTs (PMF > 1), suggesting that the complex soil moisture–precipitation coupling may be attributed to the coupling of soil moisture–latent heat flux–precipitation and soil moisture–moisture convergence–precipitation (Fig. 3j). Additionally, the soil moisture–latent heat flux–precipitation transitive chain is dominant in wet regions (i.e., humid and transitional regions), and the areas with significant soil moisture–latent heat flux–precipitation transitive chain are even twice the size of those with significant soil moisture–moisture convergence–precipitation transitive chain for ERA5 and GLEAM. However, the regions affected by the significant soil moisture–moisture convergence–precipitation transitive chain is much larger in dry regions (i.e., arid regions), accounting for about 35.94%, 26.26%, and 46.84% for ERA5,

GLEAM, and MERRA-2 (Fig. 3k), respectively. Thus, the complex soil moisture–precipitation coupling can be explained through the indirect process chains as a result of land–atmosphere feedbacks, and soil moisture–latent heat flux–precipitation and soil moisture–moisture convergence–precipitation transitive chains are likely to play a contrasting role in triggering the occurrence of DPT events over wet and dry regions.

Contribution of coupling chains to the occurrence of DPTs.

We further conduct a causal analysis using the convergent cross mapping algorithm (see Methods) to detect causal relationships of soil moisture–latent heat flux–precipitation and soil moisture–moisture convergence–precipitation transitive chains in humid, transitional, and arid regions. Generally, soil moisture dynamics force latent heat flux dynamics, and precipitation dynamics are affected by latent heat flux dynamics. Although the

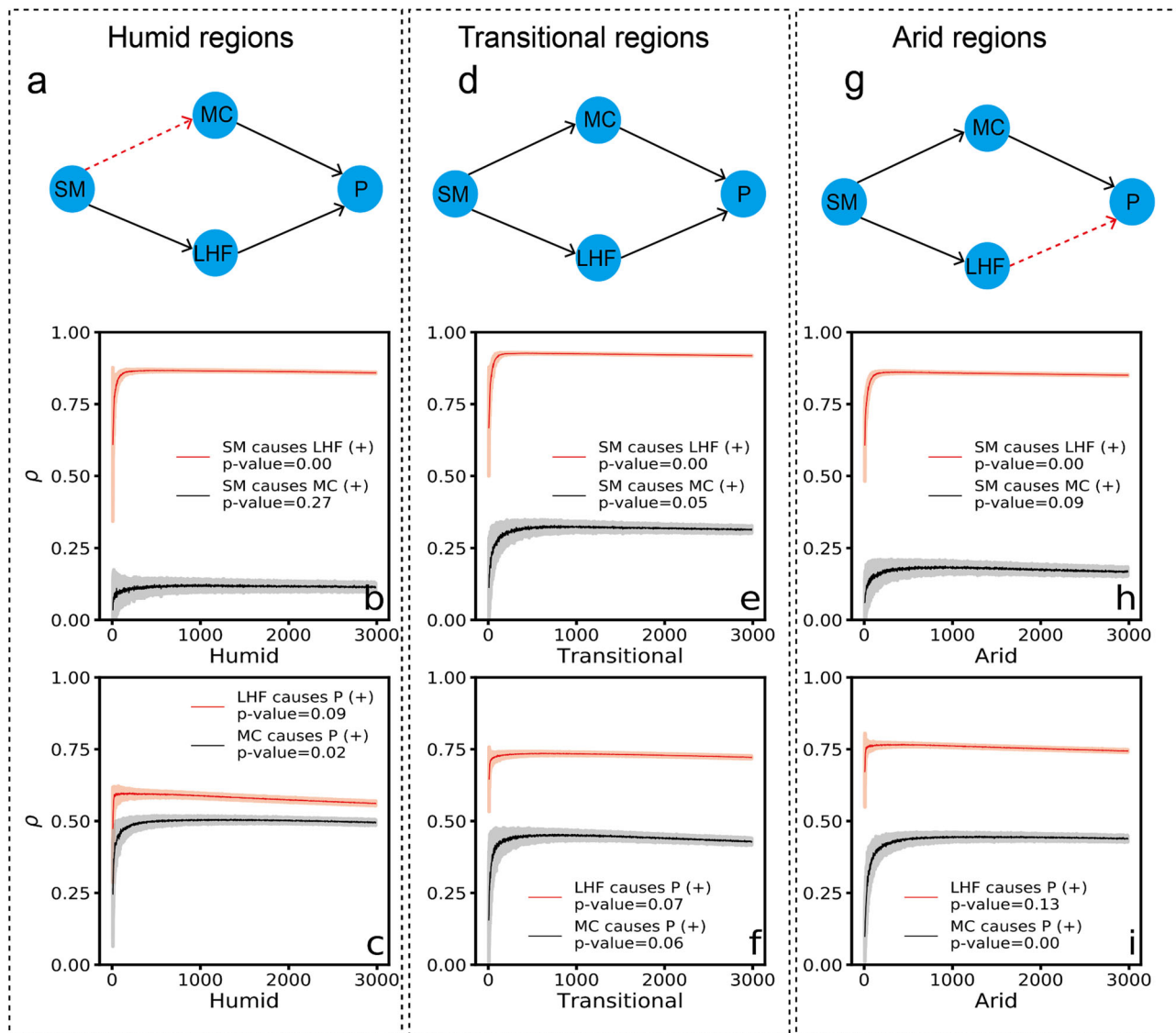


Fig. 4 Detection of causality using convergent cross mapping. **a** Direct causality in a transitive causal chain for DPTs in humid regions. **b** Causal relationships of soil moisture–latent heat flux (SM–LHF) and soil moisture–moisture convergence (SM–MC) for humid regions. **c** Causal relationships of latent heat flux–precipitation (LHF–P) and moisture convergence–precipitation (MC–P) for humid regions. **d** Direct causality in a transitive causal chain for DPTs in transitional regions. **e** Causal relationships of SM–LHF and SM–MC in transitional regions. **f** Causal relationships of LHF–P and MC–P in transitional regions. **g** Direct causality in a transitive causal chain for DPTs in arid regions. **h** Causal relationships of SM–LHF and SM–MC in arid regions. **i** Causal relationships of LHF–P and MC–P in arid regions. The black and red lines with arrow in **a**, **d**, and **g** indicate significant (p -value < 0.1) and insignificant (p -value ≥ 0.1) causal relationships, respectively. The x axis represents the time-series length. The shaded regions show mean \pm SD from bootstrapped iterations. The results are based on the mean results from ERA5, GLEAM, and MERRA-2. The plus (+) sign represents significant correlations of SM–MC, SM–LHF, MC–P, and LHF–P.

causal relationships between moisture convergence and precipitation are significant, the level of skill in the cross mapping on moisture convergence from soil moisture (Pearson correlation coefficient (ρ) = 0.17 and not significant) is much lower than that of latent heat flux from soil moisture (ρ = 0.86), indicating that compared with soil moisture–moisture convergence–precipitation, the soil moisture–latent heat flux–precipitation coupling chain contributes more to the DPTs in humid regions (Fig. 4b, c). And the soil moisture–latent heat flux–precipitation and soil moisture–moisture convergence–precipitation transitive chains all show a significant causal relationship in transitional regions (Fig. 4d, e, f). By contrast, the soil moisture–moisture convergence–precipitation coupling chain is the dominant factor causing the DPTs in arid regions (Fig. 4g). Although latent heat

flux is strongly forced by soil moisture (ρ = 0.84), the contribution of latent heat flux–precipitation coupling is not statistically significant, leading to an insignificant transitive causal chain of soil moisture–latent heat flux–precipitation in dry regions (Fig. 4h, i).

To examine whether the soil moisture–latent heat flux–precipitation and soil moisture–moisture convergence–precipitation transitive chains have a contrasting role in triggering the occurrence of DPT events over wet regions (i.e., humid and transitional regions) and dry regions (i.e., arid regions), we investigate the statistically significant change in the spatial distribution and shift in the median value of the DPTs frequencies for the regions with significant soil moisture–latent heat flux–precipitation and soil moisture–moisture convergence

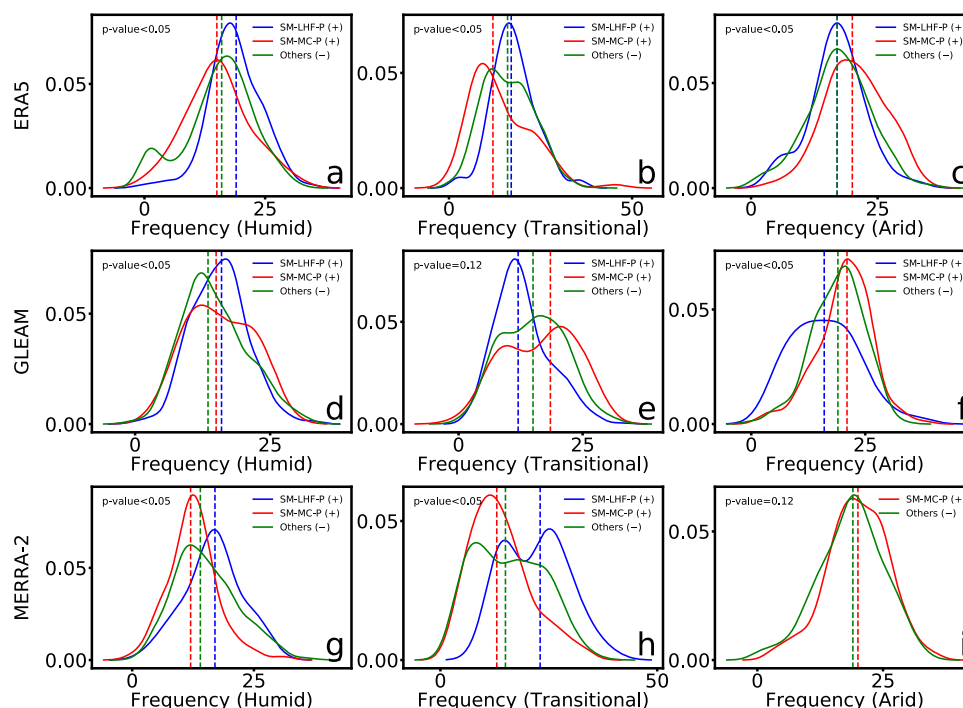


Fig. 5 Distribution of the total number of DPT for humid, transitional, and arid regions with significant soil moisture–latent heat flux–precipitation (SM–LHF–P (+)) and soil moisture–moisture convergence–precipitation (SM–MC–P (+)) transitive chains, as well as the regions without these two coupling chains (Others (–)). Probability density function represents the distribution of differences in total number of DPT events among the areas with significant soil moisture–latent heat flux–precipitation transitive chains, the areas with significant soil moisture–moisture convergence–precipitation transitive chains, and the areas without any significant transitive chain for ERA5 over **a** humid, **b** transitional, and **c** arid regions. **d–f** Same as **a–c** but for GLEAM dataset. **g–i** Same as **a–c** but for MERRA-2 dataset. The plus (+) and minus (–) signs represent significant and insignificant soil moisture–latent heat flux–precipitation and soil moisture–moisture convergence–precipitation transitive chains, respectively. The distribution of the total number of DPT events over the areas with significant soil moisture–latent heat flux–precipitation transitive chain in **i** was excluded because there were only two points which were statistically significant.

–precipitation transitive chains, as well as the regions without these two significant transitive chains. We examine the difference between the regions with different coupling chains by comparing the probability density functions of DPTs frequencies for three different datasets. The statistically significant changes in the spatial distribution and shift in the median value of DPTs frequencies are investigated using the two-sample Kolmogorov-Smirnov test. For humid regions, the spatial pattern of the DPTs frequency exhibits a significant (at 95% confidence level) positive shift in the median over the areas with significant soil moisture–latent heat flux–precipitation transitive coupling chain, and an obvious positive shift in the median can be observed for all three datasets, indicating that the areas with soil moisture–latent heat flux–precipitation coupling chain are experiencing more DPT events compared with the areas without such coupling chain (i.e., the areas with soil moisture–moisture convergence–precipitation chain and the areas without these two chains) (Fig. 5a, d, g). This confirms a substantial contribution of soil moisture–latent heat flux–precipitation coupling chain to the transition from drought to pluvial in humid regions. For transitional regions, there is no consistent positive shift in the median of DPTs frequency for all three datasets, but ERA5 and MERRA-2 witness a positive shift in the median over the areas with significant soil moisture–latent heat flux–precipitation transitive coupling chain (Fig. 5b, e, h). On the contrary, the arid regions with significant soil moisture–moisture convergence–precipitation coupling chain witness a positive shift in spatial pattern of the DPTs frequency for all three datasets. Such a consistent positive shift in the median of DPTs frequency suggests the contribution of soil moisture–moisture convergence

–precipitation transitive coupling chain to the occurrence of DPT events (Fig. 5c, f, i). Additionally, latent heat flux increases during drought compared with that during the month before the drought occurrence over humid regions, especially for Amazon Basin, Southeast Asia, and Eastern North America, further confirming the contribution of soil moisture–latent heat flux–precipitation transitive causal chain to the occurrence of rainfall following the drought in humid regions. On the other hand, the dry regions witness an obvious increase in moisture convergence during pluvial compared with that during the month before the drought occurrence, further suggesting the soil moisture–moisture convergence–precipitation chain enhancing the post-drought rainfall in dry regions (Supplementary Fig. 15).

It should be noted that extreme events can be attributable to both large-scale atmospheric dynamics and local land–atmosphere feedbacks. In this study, we focus on the land–atmosphere feedbacks and aim to confirm that the soil moisture–latent heat flux–precipitation and soil moisture–moisture convergence–precipitation coupling chains contribute to the occurrence of abrupt shift from drought to pluvial, which means that land–atmosphere feedbacks may be one of the reasons for the occurrence of DPT events. Extreme events, especially for drought to pluvial, are also associated with atmospheric phenomena (e.g., large-scale teleconnections, blocking patterns, frontal weather systems, etc.). However, atmospheric circulation anomalies are not the only cause of the most extreme compound events, which tend to trigger climate extremes and extreme low soil moisture⁴⁴. Land–atmosphere interactions can modify atmospheric dryness, cloud cover and moisture convergence and therefore the

likelihood of cloud/precipitation generation, potentially influencing the occurrence of DPT events. In the case of southeastern Australian (Millennium) drought and the subsequent rainfall event, previous studies emphasized the role of El Niño–Southern Oscillation (ENSO) on the drought and pluvial transition that occurred in Australia⁴⁵, and such a transition can also be explained from the perspective of soil moisture–moisture convergence–precipitation coupling chain (Supplementary Fig. 16). Thus, soil moisture variability induced by atmospheric circulation dynamics is necessary for the soil moisture–climate feedback, and soil moisture itself can also affect atmospheric circulation dynamics. Considering the influence of large-scale atmospheric dynamics on the land–atmosphere couplings in a more comprehensive manner can advance our understanding of the occurrence and evolution of abrupt shift from drought to pluvial.

Discussion and implications

We conduct sensitivity analysis by changing soil depths. By comparing DPTs frequencies identified by soil moisture in the top and the root-zone layers, we find that the use of top-layer soil moisture is able to capture similar hotspots as well as a significant increasing trend in the DPTs frequency compared with those using the root-zone soil moisture (Supplementary Figs. 17 and 18). However, the water stored in the root-zone layer is directly available to support transpiration and plant growth, which are key regulators of surface evaporation^{46,47}. Although surface soil moisture responds faster to dryness, the deficit in the root-zone soil moisture can directly result in a strong reduction in transpiration since soil canopy re-evaporation and soil evaporation are small^{48–50}. Thus, we identify DPTs based on the changes in the root-zone soil moisture instead of the top-layer soil moisture from the perspective of potential impacts of DPT events.

This study examines the crucial role of soil moisture–atmosphere feedbacks in promoting the occurrence of DPTs over wet and dry regions. We should also pay attention to the beneficial impact of soil moisture–atmosphere feedbacks on the hydrological cycle, particularly over drylands. The reduced soil moisture enhances moisture convergence, which partly counteracts precipitation declines driven by limited evaporation. In other words, future precipitation changes would comply with the “dry get drier” paradigm in dry regions without considering the soil moisture–atmosphere feedbacks. Due to the existing soil moisture–atmosphere feedbacks, however, the increased moisture convergence induced by the decreased soil moisture may partially offset the decline in moisture over drylands¹⁸, which plays an important role in global water cycle. On the other hand, the contribution of soil moisture–atmosphere feedbacks to rainfall would favor the “wet get wetter” paradigm in wet regions. Although extreme precipitation does not always lead to flooding due to the dry soil moisture modulation of flood response, the wet areas are more likely to experience more widespread floods due to the occurrence of heavy rainfall after droughts⁵¹.

The crucial role of soil moisture–atmosphere feedbacks in promoting DPTs also has important implications for the occurrence of flash drought and subsequent rainfall, which occur at shorter timescales than compound drought and rainfall events assessed in this study. Specifically, flash droughts and heavy rainfall are short-term and intense extreme events, such as sub-seasonal flash droughts followed by heavy rains. Thus, there is less time for impact preparation, potentially causing more severe impacts on the environment and society. Investigating the soil moisture–atmosphere interactions can also advance the understanding of physical mechanisms causing the shift from flash drought to heavy rainfall over relatively short timescales, thereby

facilitating the development of early warning systems for mitigating the impacts of such rapid shifts.

Our study identifies the critical regions of DPTs and reveals the underlying mechanisms triggering the abrupt transition between drought to pluvial. According to our analysis using reanalysis datasets, the magnitudes and frequencies of DPTs are enhanced in the regions with strong soil moisture–atmosphere feedbacks, which has important implications for advancing understanding of hydroclimatic variability. Our findings can provide meaningful information for policymakers and stakeholders to realize global hotspots that are expected to experience more DPTs in a changing climate. More importantly, revealing the contribution of soil moisture–atmosphere feedbacks to the DPTs enables us to pay more attention to the regions with strong soil moisture–atmosphere feedbacks, which will not only support forecasting efforts but also facilitate hazard preparedness and mitigation planning.

Methods

Identification of the DPT. We focus on the contribution of soil moisture–atmosphere feedbacks to the drought and pluvial transitions (DPTs), that is, the shift from drought (soil moisture deficit) to pluvial (enhanced precipitation). We use standardized metrics to compare drought and pluvial events over time and space. As for the drought assessment, the standardized soil moisture index (SSI⁵²) is adopted based on soil moisture. Similarly, the pluvial is identified using the standardized precipitation index calculated based on precipitation (SPI⁵³). Although there are other indicators available for monitoring and analyzing drought and pluvial, the transitive relations between soil moisture and precipitation behind the DPTs are the focus of this study, and thus we choose the SSI and SPI to identify drought and pluvial, respectively. Specifically, SSI and SPI were determined for every grid independently throughout the same pentad for each year over the period of 1980–2020, to enable a comparison of relatively drought and pluvial throughout the same time every year, which can avoid the influence of seasonal changes and different climate zones. More details of SSI and SPI calculations can be found in Supplementary Methods, and the climatic water condition based on SPI and SSI can be divided into seven grades, as shown in Supplementary Tables 1 and 2. DPTs represents drought abruptly shift to pluvial in adjacent pentads, and in order to avoid the influence of natural buffers and the resilience in soil moisture levels, drought events should last at least 3 pentads (15 days).

Detection of causal relationships. Convergent cross mapping is a powerful methodological approach that can help distinguish causality from spurious correlation in time series of non-linear dynamical systems^{54,55}. In convergent cross mapping, causality is detected by measuring the extent to which the historical record of the affected variable Y (or its proxies) reliably estimates the states of a causal variable X . That is, if variable X is influencing Y , then, based on the generalized Takens’ theorem, the causal variable X can be recovered from the historical record of the affected variable Y . The skill of cross mapping is defined as the correlation coefficient ρ between predictions and observations of X . If the ρ increases with the length of the time series and convergence is present, then the causal effect of X on Y can be inferred. A simple model system consisting of 2 coupled logistic difference equations can be expressed as

$$X(t+1) = X(t)(r_x - r_x X(t) - \beta_{x,y} Y(t)) \quad (1)$$

$$Y(t+1) = Y(t)(r_y - r_y Y(t) - \alpha_{y,x} X(t)) \quad (2)$$

where t and $t+1$ are the time steps. r_x and r_y are the variables’ intrinsic growth rates, and $\beta_{x,y}$ and $\alpha_{y,x}$ represent the impacts of variable X on the dynamics of variable Y and the impacts of variable Y on the dynamics of variable X , respectively.

In this study, the convergent cross mapping analysis was implemented using the multispatialCCM package in the R language environment. We analyze dynamical systems using optimal embedding dimension estimated by simplex projection, and $\tau = 1$ (time lags), iterations = 500 (the number of bootstrap iterations) based on pentad data for the study period.

Detection of temporal trends. The Mann–Kendall (MK)^{56,57} method is a non-parametric test, which has been commonly used for trend detection by examining whether there is a monotonic trend in the time series of the variable of interest. A positive value of standardized test statistic Z_{MK} indicates an increasing trend in the time series of DPTs, whereas a negative Z_{MK} value suggests a decreasing trend. The advantage of this method is that samples are not required to follow a particular distribution. Thus, this method is not affected by a few abnormal values, and can be used to well characterize the trend of a time series. The MK trend analysis was performed in this study to examine the trend of DPTs on a global scale. For a given

time series (x_1, \dots, x_n) , the test statistic Z_{MK} was calculated as follows:

$$S = \sum_{i=1}^{n-1} \sum_{j=i+1}^n \text{sign}(x_j - x_i) \quad (3)$$

$$\text{sign}(x_j - x_i) = \begin{cases} +1, & x_j > x_i \\ 0, & x_j = x_i \\ -1, & x_j < x_i \end{cases} \quad (4)$$

$$\text{Var}(S) = \frac{1}{18} \left[n(n-1)(2n+5) - \sum_p t_p(t_p-1)(2t_p+5) \right] \quad (5)$$

$$Z_{MK} = \begin{cases} \frac{S-1}{\sqrt{\text{Var}(S)}} & \text{if } S > 0 \\ 0 & \text{if } S = 0 \\ \frac{S+1}{\sqrt{\text{Var}(S)}} & \text{if } S < 0 \end{cases} \quad (6)$$

where n is the length of the time series. x_i and x_j are the sequential data in time series. t_p is the number of ties of the p_{th} value.

Bivariate copulas and probability multiplication factor (PMF). The bivariate copulas are mathematical functions that can be used to describe the dependence between two random variables and to derive their joint distribution. The main advantage of the copula is its ability to overcome the shortcoming of assessing the co-occurrence frequency of two climate extremes with few samples⁵⁸. The joint distribution of random variables X and Y can be expressed as

$$F_{X,Y}(x, y) = P(X \leq x, Y \leq y) \quad (7)$$

where X and Y are random variables, and P is their joint distribution. $F_X(x) = P(X \leq x)$ and $F_Y(y) = P(Y \leq y)$ are the marginal probability distribution of X and Y , respectively. The joint cumulative distribution function (CDF) of X and Y can be expressed as

$$F_{X,Y}(x, y) = C[F_X(x), F_Y(y)] = C(u, v), 0 \leq u, v \leq 1 \quad (8)$$

where $F_X(x)$ and $F_Y(y)$ are transformed into two uniformly distributed random variables u and v , and C is a copula function. The copula families, including Gaussian, Student's t , Clayton, Gumbel, and Frank copula, were used to model the dependence structures of random variables. For each grid point, the optimal copula model was selected based on the Bayesian Information Criterion to well represent the dependence structure between two random variables.

In this study, we assess the joint probabilities of extreme soil moisture –precipitation at different thresholds. For example, to assess the joint probability of drought (soil moisture (SM) below the 15th percentile) and next pentad pluvial (precipitation (P) above the 85th percentile), the probability of such a compound event can be calculated as

$$p = P(u < 0.15 \cap v > 0.85) = P(u < 0.15) - P(u < 0.15 \cap v \leq 0.85) = 0.15 - C(0.15, 0.85) \quad (9)$$

Calculation and decomposition of moisture convergence. Atmospheric moisture convergence (MC) is calculated as the negative divergence of vertically integrated moisture flux over the pressure (P) from the top of the atmosphere ($P = 0$) to the surface ($P = P_s$).

$$MC = -\frac{1}{\rho_w g} \nabla \cdot \int_0^{P_s} (uq) dp \quad (10)$$

where ρ_w is the density of water, g is the acceleration due to gravity, ∇ is the horizontal divergence operator, u is the horizontal vector wind and q is specific humidity.

At a pentad scale, moisture convergence can be decomposed into thermodynamic (TH) component determined by specific humidity anomalies and mean circulation dynamic (MCD) component determined by horizontal wind anomalies.

$$\delta TH = -\frac{1}{\rho_w g} \nabla \cdot \int_0^{P_s} (u\delta q) dp \quad (11)$$

$$\delta MCD = -\frac{1}{\rho_w g} \nabla \cdot \int_0^{P_s} (q\delta u) dp \quad (12)$$

The subscript 'δ' represents departure from the pentad climatology.

Definition of dryland. The global arid, transitional, and humid regimes can be identified as regions with an aridity index (AI)⁵⁹. The aridity index (AI), expressed as the ratio of potential evaporation (Ep) to precipitation (P), is a widely used indicator of regional moisture conditions. It is an effective index used to classify arid, transitional, and humid zones (Supplementary Fig. 19). The interplay between water supply and demand, including both precipitation and potential evaporation, is critical to the assessment of changes in dryness and dryland dynamics. The AI

can thus be calculated based on the ratio between average annual potential evaporation and precipitation using monthly potential evaporation and precipitation data from the Climatic Research Unit (CRU), which represents the characteristics of dryness/desertification over a specific region.

$$AI = \frac{Ep}{P} \begin{cases} \text{arid} (AI > 2.25) \\ \text{transitional} (0.9 < AI \leq 2.25) \\ \text{humid} (AI \leq 0.9) \end{cases} \quad (13)$$

Data availability

Daily root-zone soil moisture and precipitation were obtained from the European Centre for Medium-Range Weather Forecasts (ERA5) (<https://www.ecmwf.int/en/forecasts/datasets/reanalysis-datasets/era5>), the Modern-Era Retrospective Analysis for Research and Applications, version 2 (MERRA-2) (<https://disc.gsfc.nasa.gov>), and the Global Land Evaporation Amsterdam Model (GLEAM) (<https://www.gleam.eu/>) and the Multi-Source Weighted Ensemble Precipitation (MSWEP) (<https://gwadi.org/multi-source-weighted-ensemble-precipitation-mswep>) datasets. The datasets used to reproduce the methods and findings of this study are available at <https://doi.org/10.5281/zenodo.8085169>.

Code availability

The code used for this study is available at <https://doi.org/10.5281/zenodo.8085169>.

Received: 2 February 2023; Accepted: 4 July 2023;

Published online: 13 July 2023

References

- Flanagan, P. X. et al. Primary atmospheric drivers of pluvial years in the United States Great Plains. *J. Hydrometeorol.* **19**, 643–658 (2018).
- He, X. & Sheffield, J. Lagged compound occurrence of droughts and pluvials globally over the past seven decades. *Geophys. Res. Lett.* **47**, e2020GL087924 (2020).
- Martin, E. R. Future projections of global pluvial and drought event characteristics. *Geophys. Res. Lett.* **45**, 11,913–11,920 (2018).
- Kourgialas, N. N. Hydroclimatic impact on mediterranean tree crops area—Mapping hydrological extremes (drought/flood) prone parcels. *J. Hydrol.* **596**, 125684 (2021).
- Venkatappa, M. et al. Impacts of droughts and floods on croplands and crop production in Southeast Asia—An application of Google Earth Engine. *Sci. Total Environ.* **795**, 148829 (2021).
- Lu, E. et al. The atmospheric anomalies associated with the drought over the Yangtze River basin during spring 2011. *J. Geophys. Res. Atmos.* **119**, 5881–5894 (2014).
- Otkin, J. A. et al. Flash droughts: a review and assessment of the challenges imposed by rapid onset droughts in the United States. *Bull. Amer. Meteor. Soc.* **99**, 911–919 (2018).
- Yoon, J. H., Wang, S. Y. S. Lo, M. H. & Wu, W. Y. Concurrent increases in wet and dry extremes projected in Texas and combined effects on groundwater. *Environ. Res. Lett.* **13**, 054002 (2018).
- Trenberth, K. E., Dai, A., Rasmussen, R. M. & Parsons, D. B. The changing character of precipitation. *Bull. Am. Meteorol. Soc.* **84**, 1205–1218 (2003).
- Giorgi, F. et al. Higher hydroclimatic intensity with global warming. *J. Clim.* **24**, 5309–5324 (2011).
- Collet, L., Harrigan, S., Prudhomme, C., Formetta, G. & Beevers, L. Future hot-spots for hydro-hazards in Great Britain: A probabilistic assessment. *Hydrol. Earth Syst. Sci.* **22**, 5387–5401 (2018).
- Koster, R. D. et al. Regions of strong coupling between soil moisture and precipitation. *Science* **305**, 1138–1140 (2004).
- Koster, R. D. et al. GLACE: the global land-atmosphere coupling experiment. Part I: overview. *J. Hydrometeorol.* **7**, 590–610 (2006).
- Findell, K. L. et al. Probability of afternoon precipitation in eastern United States and Mexico enhanced by high evaporation. *Nature Geosci.* **4** 434–439 (2011).
- D'Odorico, P. & Porporato, A. Preferential states in soil moisture and climate dynamics. *PNAS* **101**, 8848–8851 (2004).
- Ruiz-Barradas, A. & Nigam, S. Warm season rainfall variability over the U.S. Great plains in observations, NCEP and ERA-40 reanalyses, and NCAR and NASA atmospheric model simulations. *J. Clim.* **18**, 1808–1830 (2005).
- Guo, L. et al. The contributions of local and remote atmospheric moisture fluxes to East Asian precipitation and its variability. *Clim. Dyn.* **51**, 4139–4156 (2018).

18. Zhou, S. et al. Soil moisture–atmosphere feedbacks mitigate declining water availability in drylands. *Nat. Clim. Chang.* **11**, 38–44 (2021).
19. Alizadeh, M. R. et al. A century of observations reveals increasing likelihood of continental-scale compound dry-hot extremes. *Sci. Adv.* **6**, eaaz4571 (2020).
20. Hao, Z. et al. Impact of dependence changes on the likelihood of hot extremes under drought conditions in the United States. *J. Hydro.* **581**, 124410 (2020).
21. Wang, R. et al. Likelihood of compound dry and hot extremes increased with stronger dependence during warm seasons. *Atmos. Res.* **260**, 105692 (2021).
22. IPCC Climate Change 2021: The Physical Science Basis Contribution of Working Group I to the Sixth Assessment Report of the Intergovernmental Panel on Climate Change Technical report. <https://www.ipcc.ch/report/sixth-assessment-report-working-group-i/> (2021).
23. Dai, A., Trenberth, K. E. & Karl, T. R. Global variations in droughts and wet spells: 1900–1995. *Geophys. Res. Lett.* **25**, 3367–3370 (1998).
24. Woodhouse, C. A. et al. The twentieth-century pluvial in the western United States. *Geophys. Res. Lett.* **32**, L07701 (2005).
25. Seager, R. et al. Modeling of tropical forcing of persistent droughts and pluvials over western North America: 1856–2000. *J. Clim.* **18**, 4065–4088 (2005).
26. Tolika, K. & Maheras, P. Spatial and temporal characteristics of wet spells in Greece. *Theor. Appl. Climatol.* **81**, 71–85 (2005).
27. Tammets, T. Distribution of extreme wet and dry days in Estonia in last 50 years. *Proc. Estonian Acad. Sci. Eng.* **13**, 252–259 (2007).
28. Findell, K. L. & Delworth, T. L. Impact of common sea surface temperature anomalies on global drought and pluvial frequency. *J. Clim.* **23**, 485–503 (2010).
29. Zolina, O., Simmer, C., Gulev, S. K. & Kollet, S. Changing structure of European precipitation: longer wet periods leading to more abundant rainfalls. *Geophys. Res. Lett.* **37**, L06704 (2010).
30. Zhang, B., Wang, S. & Wang, Y. Copula-based convection-permitting projections of future changes in multivariate drought characteristics. *J. Geophys. Res. Atmos.* **124**, 7460–7483 (2019).
31. Chen, H., Wang, S. & Wang, Y. Exploring abrupt alternations between wet and dry conditions on the basis of historical observations and convection-permitting climate model simulations. *J. Geophys. Res. Atmos.* **125**, e2019JD031982 (2020).
32. Miralles, D. G., Teuling, A. J., Van Heerwaarden, C. C. & Vilà-Guerau de Arellano, J. Mega-heatwave temperatures due to combined soil desiccation and atmospheric heat accumulation. *Nat. Geosci.* **7**, 345–349 (2014).
33. Berg, A. et al. Land–atmosphere feedbacks amplify aridity increase over land under global warming. *Nat. Clim. Chang.* **6**, 869–874 (2016).
34. Koster, R. D., Chang, Y., Wang, H. & Schubert, S. D. Impacts of local soil moisture anomalies on the atmospheric circulation and on remote surface meteorological fields during boreal summer: a comprehensive analysis over North America. *J. Clim.* **29**, 7345–7364 (2016).
35. Berg, A., Lintner, B., Findell, K. & Giannini, A. Soil moisture influence on seasonality and large-scale circulation in simulations of the West African monsoon. *J. Clim.* **30**, 2295–2317 (2017).
36. Zampieri, M. et al. Hot European summers and the role of soil moisture in the propagation of Mediterranean drought. *J. Clim.* **22**, 4747–4758 (2009).
37. Jaeger, E. B. & Seneviratne, S. I. Impact of soil moisture–atmosphere coupling on European climate extremes and trends in a regional climate model. *Clim. Dyn.* **36**, 1919–1939 (2011).
38. Saini, R., Wang, G. & Pal, J. S. Role of soil moisture feedback in the development of extreme summer drought and flood in the United States. *J. Hydrometeorol.* **17**, 2191–2207 (2016).
39. Wei, J., Su, H. & Yang, Z. L. Impact of moisture flux convergence and soil moisture on precipitation: a case study for the southern United States with implications for the globe. *Clim. Dyn.* **46**, 467–481 (2016).
40. Allan, R. P. & Soden, B. J. Atmospheric warming and the amplification of precipitation extremes. *Science* **321**, 1481–1484 (2008).
41. O’Gorman, P. A. & Schneider, T. The physical basis for increases in precipitation extremes in simulations of 21st-century climate change. *PNAS* **106**, 14773–14777 (2009).
42. O’Gorman, P. A. Sensitivity of tropical precipitation extremes to climate change. *Nature Geosci.* **5**, 697–700 (2012).
43. Roderick, T. P., Wasko, C. & Sharma, A. Atmospheric moisture measurements explain increases in tropical rainfall extremes. *Geophys. Res. Lett.* **46**, 1375–1382 (2019).
44. Zhou, S. et al. Land–atmosphere feedbacks exacerbate concurrent soil drought and atmospheric aridity. *PNAS* **116**, 18848–18853 (2019).
45. King, A. D. et al. The role of climate variability in Australian drought. *Nat. Clim. Chang.* **10**, 177–179 (2020).
46. Rengasamy, P., Chittleborough, D. & Helyar, K. Root-zone constraints and plant-based solutions for dryland salinity. *Plant Soil* **257**, 249–260 (2003).
47. Champagne, C. et al. Evaluation of soil moisture extremes for agricultural productivity in the Canadian prairies. *Agric. For. Meteorol.* **165**, 1–11 (2012).
48. Or, D. et al. Advances in soil evaporation physics—a review. *Vadose Zone J.* **12**, 1–16 (2013).
49. Brutsaert, W. & Chen, D. Desorption and the two stages of drying of natural tallgrass prairie. *Water Resour. Res.* **31**, 1305–1313 (1995).
50. Brutsaert, W. Daily evaporation from drying soil: universal parameterization with similarity. *Water Resour. Res.* **50**, 3206–3215 (2014).
51. Sharma, A., Wasko, C. & Lettenmaier, D. P. If precipitation extremes are increasing, why aren’t floods? *Water Resour. Res.* **54**, 8545–8551 (2018).
52. Hao, Z. & AghaKouchak, A. Multivariate Standardized Drought Index: a multi-index parametric approach for drought analysis. *Adv. Water Resour.* **57**, 12–18 (2013).
53. McKee, T. B., Doesken, N. J. & Kleist, J. The relationship of drought frequency and duration to time scales. In *8th Conference on Applied Climatology* 17, 179–183 (Anaheim, California, American Meteorological Society, 1993).
54. Sugihara, G. et al. Detecting causality in complex ecosystems. *Science* **338**, 496–500 (2012).
55. Clark, A. T. et al. Spatial convergent cross mapping to detect causal relationships from short time series. *Ecology* **96**, 1174–1181 (2015).
56. Mann, H. B. Nonparametric tests against trend. *Econometrica* **13**, 245–259 (1945).
57. Kendall, M. G. *Rank Correlation Methods*, 272 (Griffin, 1975).
58. Zscheischler, J. & Seneviratne, S. I. Dependence of drivers affects risks associated with compound events. *Sci. Adv.* **3**, e1700263 (2017).
59. Rienecker, M. M. et al. MERRA: NASA’s modern-era retrospective analysis for research and applications. *J. Clim.* **24**, 3624–3648 (2011).

Acknowledgements

S.W. acknowledges support from the Hong Kong Research Grants Council Early Career Scheme (grant no. 25222319) and the Hong Kong Polytechnic University (grant no. P0045957, P0043040).

Author contributions

S.W. conceived and supervised the study. Y.Q. and S.W. carried out the analysis and wrote the paper. Y.Q. and S.W. contributed equally to this work. Z.L.Y. and P.G. provided comments and suggestions for improving the quality of this paper.

Competing interests

The authors declare no competing interest.

Additional information

Supplementary information The online version contains supplementary material available at <https://doi.org/10.1038/s43247-023-00922-2>.

Correspondence and requests for materials should be addressed to Shuo Wang.

Peer review information *Communications Earth & Environment* thanks the anonymous reviewers for their contribution to the peer review of this work. Primary Handling Editors: Akintomide Akinsanola and Aliénor Lavergne. A peer review file is available.

Reprints and permission information is available at <http://www.nature.com/reprints>

Publisher’s note Springer Nature remains neutral with regard to jurisdictional claims in published maps and institutional affiliations.



Open Access This article is licensed under a Creative Commons Attribution 4.0 International License, which permits use, sharing, adaptation, distribution and reproduction in any medium or format, as long as you give appropriate credit to the original author(s) and the source, provide a link to the Creative Commons license, and indicate if changes were made. The images or other third party material in this article are included in the article’s Creative Commons license, unless indicated otherwise in a credit line to the material. If material is not included in the article’s Creative Commons license and your intended use is not permitted by statutory regulation or exceeds the permitted use, you will need to obtain permission directly from the copyright holder. To view a copy of this license, visit <http://creativecommons.org/licenses/by/4.0/>.

© The Author(s) 2023